Taylor & Francis
Taylor & Francis Group

SHORT REPORT

Intravital characterization of tumor cell migration in pancreatic cancer

Evelyne Beerling[a,‡], Ilse Oosterom[b,‡], Emile Voest[c,†], Martijn Lolkema[b,†,‡], and Jacco van Rheenen[a,‡]

[a]Cancer Genomics Netherlands, Hubrecht Institute-KNAW & University Medical Center Utrecht, Utrecht, the Netherlands; [b]University Medical Center Utrecht, Utrecht, the Netherlands; [c]Cancer Genomics Netherlands, The Netherlands Cancer Institute, Amsterdam, the Netherlands

ABSTRACT
Curing pancreatic cancer is difficult as metastases often determine the poor clinical outcome. To gain more insight into the metastatic behavior of pancreatic cancer cells, we characterized migratory cells in primary pancreatic tumors using intravital microscopy. We visualized the migratory behavior of primary tumor cells of a genetically engineered pancreatic cancer mouse model and found that pancreatic tumor cells migrate with a mesenchymal morphology as single individual cells or collectively as a stream of non-cohesive single motile cells. These findings may improve our ability to conceive treatments that block metastatic behavior.

Pancreatic cancer is one of the deadliest malignant diseases due to its propensity to metastasize. Therefore, understanding the process of metastasis formation is essential to improve patient outcome. To gain knowledge on the limiting steps of this deadly process, metastatic pancreatic cancer has been extensively studied in genetically engineered mouse models (GEMMs).[1,2] Although tumor progression to a carcinoma stage is often seen as a limiting step for dissemination and metastasis formation, experiments in pancreatic cancer mouse models showed that circulating tumor cells can be detected even in mice that display only pre-cancerous lesions.[3] The ability of tumor cells to undergo epithelial-to-mesenchymal transition (EMT) is another often thought limiting process of metastasis, however blocking EMT did not result in obliteration of metastasis formation, but instead sensitized pancreatic tumors to chemotherapy treatment.[4] Thus, developing a better insight into the inefficient and multiple step process in which cells acquire the various traits necessary for metastasis formation could aid in developing rational treatment strategies to treat or prevent metastasis formation of pancreatic tumors.[5,6]

The first rate limiting step in pancreatic cancer metastasis is the ability of tumor cells to become motile by detaching from neighbors and escaping from the primary tumor,[7–9] but this step has not yet been directly studied *in vivo*. Intravital microscopy (IVM) studies in other tumor models showed that few cells in the tumor display motile behavior and these motile cells employ different migratory strategies:[10,11] mesenchymal migration, in which cells have an elongated shape with cell polarity; bleb-driven amoeboid-like, in which cells have a less defined polarity and a more rounded shape; collective streaming migration, in which multiple cells migrate in streams of single mesenchymal cells that lack cell-cell contact, and collective cell migration, in which cells migrate as a compact multicellular group in which the adherens junctions are still intact. As pancreatic cancer is known for its aggressiveness this study aims to visualize the migratory strategies of pancreatic cancer cells using IVM.

To characterize how pancreatic tumor cells escape from the primary tumor, here we intravitally imaged a genetic fluorescent mouse model which develops fluorescent metastatic pancreatic cancer. Trp53 and KRAS are the main genes involved in the development,

CONTACT Martijn Lolkema ✉ m.lolkema@erasmusmc.nl 🖅 Erasmus MC, Department of Medical Oncology, groene Hilledijk 301, 3075 EA, Rotterdam, the Netherlands; Jacco van Rheenen ✉ j.vanrheenen@hubrecht.eu 🖅 Hubrecht Institute, Uppsalalaan 8, 3584CT, Utrecht, the Netherlands.

[†]Current address, Erasmus Medical Center Cancer Center, Erasmus Medical Center Rotterdam, the Netherlands.
[‡]These authors contributed equally to this work.

maintenance and progression of pancreatic cancer and are mutated in the majority of cases.[12–14] Conditional mouse models have been developed in which Trp53 and KRAS were genetically mutated or depleted.[1] In our study, we use a mouse model in which the expression of a non-functional Trp53 gene in both Trp53 alleles[2] and the expression of a mutant Kras (G12D) are induced by a Cre that is expressed specifically in the pancreas by the pdx-1 promotor.[15] These pdx-1-Cre;Kras[LSL-G12D/+];Trp53[LSL-R172H/FLOX] (KP[F/M]C) mice develop pancreatic ductal adenocarcinomas within ~30 d. Although these tumors develop much faster than other reported pancreatic cancer mouse models,[1] histologically these tumors are similar to their slower counterparts and to human pancreatic cancer.[15] In order to characterize migration in our model for pancreatic cancer, we labeled all tumor cells with yellow fluorescent protein (YFP) by crossing KP[F/M]C mice

with a STOP-floxed R26-YFP mouse (Fig. 1A). In these KP[F/M]C-YFP mice, after ~50 d fluorescent tumors had formed throughout the entire pancreas.

To intravitally visualize these fluorescent pancreatic cancers, we surgically exposed the pancreas by making a ~1 cm incision into the skin and abdominal wall. The mouse was placed in a custom-designed imaging box[16] and the pancreas was placed on a coverslip while still attached to the circulation. The circulation is still intact as indicated by the blood flow upon injection of 70 k$_D$ fluorescent Dextran (boxed areas in Movie S1). This setup allows for intravital imaging of pancreatic tumor tissue over a course of several hours.[17] We intravitally imaged these fluorescent pancreatic cancers by visualizing the YFP tumor cells and the collagen I using second harmonic generation (SHG) imaging. Autofluorescence signal did not interfere with our YFP detection, since the YFP fluorescence
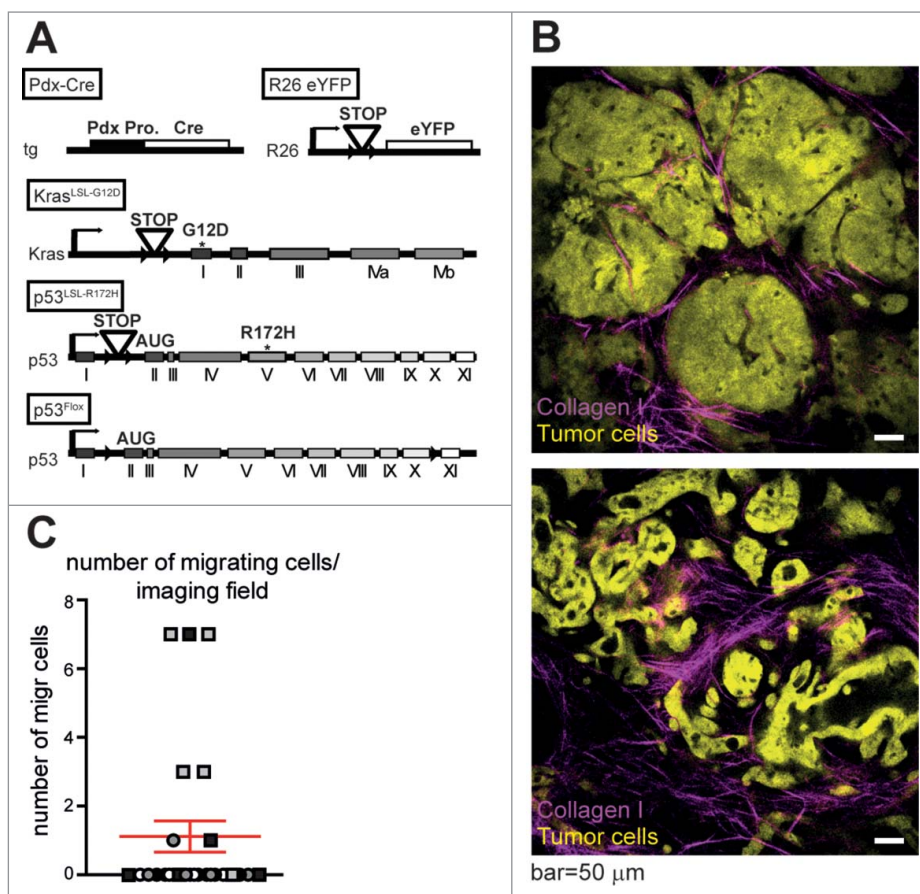
Figure 1. (A)genetic fluorescent mouse model of pancreatic cancer. (A) Schematic representation of the fluorescent mouse model in which all tumor cells express YFP upon recombination by Cre recombinase under the Pdx-promotor. In these cells, Cre-regulated mutated forms of Kras (Kras[LSL-G12D]) and p53 (p53[LSL-R172H]), combined with a floxed p53 give rise to pancreatic tumors. (B) Representative intravital microscopy images showing different types of tumor morphology in yellow and surrounding collagen I in magenta. Scale bar, 50 μm. (C) The number of migrating cells per imaging field (n = 26 fields in 5 animals). The 5 different animals are shown in symbols with different shapes/colors. Mean ± SEM.

signal of tumor cells is several orders of magnitude higher than the autofluorescence signal of non-fluorescent tumors (Fig. S1). In 5 mice, we took Z-stacks of 24 images with a Z step size of 3 μm of 5 to 9 imaging fields (0.7×0.7 mm) every 15 minutes for 2 hours. We observed that the YFP-labeled tumors consisted of tumor lobes with heterogeneous morphologies; the normal pancreatic architecture was completely replaced by tumor lobes (Fig. 1B, upper image) although some of these lobes still contained a lumen (Fig. 1B, lower image) as can be found in the healthy pancreas. Most of these tumor lobes were encapsulated by collagen, however this encapsulation was not intact in some areas (dotted lines in Fig. S2).

To characterize tumor cell migration, we visualized the cells that migrate away from the tumor lobes and invade into the healthy stroma (Fig. 2 and Movie S2). As reported previously for other models,[18,19] we found that the migratory behavior of tumor cells is very heterogeneous in these genetic pancreatic cancers tumors. In 2 out of 5 imaged mice, none of the imaging fields contained migratory tumor cells that invaded into the stroma (total of 11 imaging fields, Fig. 1C). In the other 3 mice, we observed in 7 out of 15 imaging fields tumor cells that escaped from the lobes (Fig. 1C). However, it is important to emphasize that even in the imaging fields where many migratory cells were found, the vast majority of cells did not invade into the healthy stroma
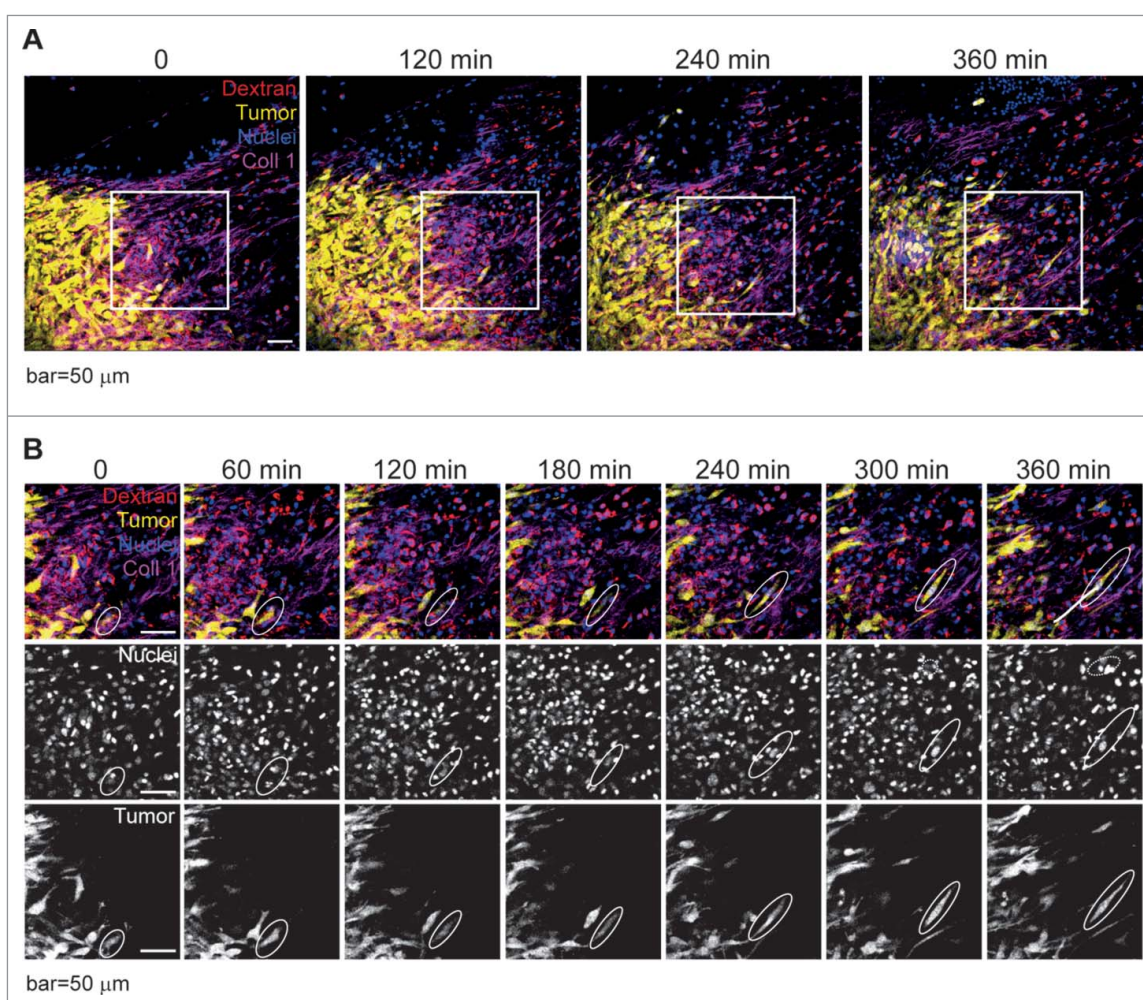
Figure 2. Tumor cells of pancreatic carcinoma migrate as mesenchymal cells. Time-lapse intravital imaging of a fluorescent mouse model of pancreatic cancer with tumor cells shown in yellow, collagen I in magenta, intravenously injected 70 k$_D$ Dextran in red and nuclei in blue. (A) Example of an imaging field (showing 4 time points (120 minute interval)), in which polar and elongated single cell migration was observed (boxed area is enlarged in B). Scale bar, 50 μm. (B) Boxed area in (A)showing an example of an imaging field (7 timepoints (60 minute interval) with migrating polar and elongated single tumor cells (example in circle) with a track (last timepoint, white line). Separate channels show the nuclei (Hoechst) and tumor cells (YFP), indicating that the particles that migrate contain nuclei. Scale bar, 50 μm.
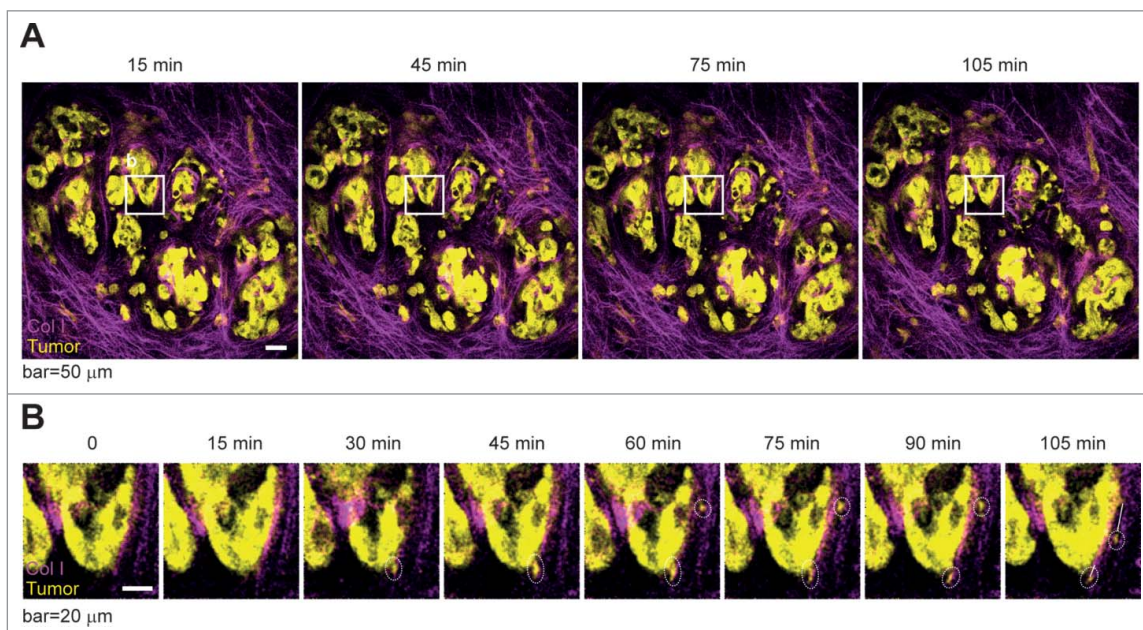
Figure 3. Single tumor cell migration in pancreatic carcinoma. Time-lapse intravital imaging of a genetic fluorescent mouse model of pancreatic cancer with tumor cells shown in yellow and collagen I in magenta. (A) Example of an imaging field (showing 4 time points (30 minute interval)), in which polar and elongated single cell migration was observed (boxed area is enlarged in B). Scale bar, 50 μm. (B) Boxed area in (A)showing migrating polar and elongated single tumor cells (in dashed circles) with a track (last time point, white line). Scale bar, 20 μm.

(Fig. 3A, Movie S3). The majority of these migratory cells migrated as polar and elongated single cells (69%, Fig. 3B and S3A, Movie S4 and S5), while the other cells migrated collectively as a stream of polar and elongated single cells (31%, Fig. 4A and B, Fig. S3B and S4, Movie S6–10). The observed migration was highly persistent (0.676+/−0.035, Fig. 4C, left graph) (persistence for random migration is 0.365[20]). Polar cells that migrate with high persistency are often referred to as having mesenchymal migratory behavior.[10] In line with this observation, the migration velocity was 14.04 ± 0.98 μm per hour (Fig. 4D, right graph), which is in the same order of mesenchymal migration observed in other mouse models and much slower than fast amoeboid migration (∼10 μm per minute[10,21–23]). Moreover, similar to different types of immune cells, amoeboid cells have a high degree of circularity (e.g. ∼0.7 for monocytes[24] and other CD45^{high} immune cells[25]) and an aspect ratio of less than[2,24,26–30] while the migratory cells that we observe have an average circularity of 0.54 ± 0.025 (Fig. 4D, left graph) and an average aspect ratio of 3.19 ± 0.226 (Fig. 4D, right graph). The latter observation confirms the notion that the observed migratory cells have a mesenchymal characteristics and not amoeboid characteristics. Collective migration of a compact multicellular group of cells, in which the adherens junctions are intact,[10,11,31,32] was not observed. Combined, these results suggest that although pancreatic tumor cells derive from an epithelial lineage, they preferably migrate as mesenchymal cells.

Here, we have characterized the first step of the metastatic cascade of pancreatic cancers by visualizing cell migration *in vivo*. Although pancreatic cancer is described as one of the most aggressive tumor types, our study shows that the vast majority of tumor cells do not escape from tumor lobes and that the few motile cells that invade into the stroma adapt a migratory strategy similar to migration strategies adapted by tumor cells in other mouse models. Our observation that cells adapt differential migration strategies (collective streaming vs single cell migration) at various imaging sites is most likely reflecting variations in the tumor microenvironment.[3] Indeed a number of studies show that variations in tumor microenvironment may change the behavior of pancreatic tumor cells, such as their response to chemotherapy.[2,33] For example, depletion of tumor stroma by using modified hyaluronidase treatment or by inhibition of sonic hedgehog signaling increased survival of mice treated with gemcitabine.[2,33] Targeting the tumor microenvironment can also make tumors more aggressive.[34] Combined our data suggest that to understand
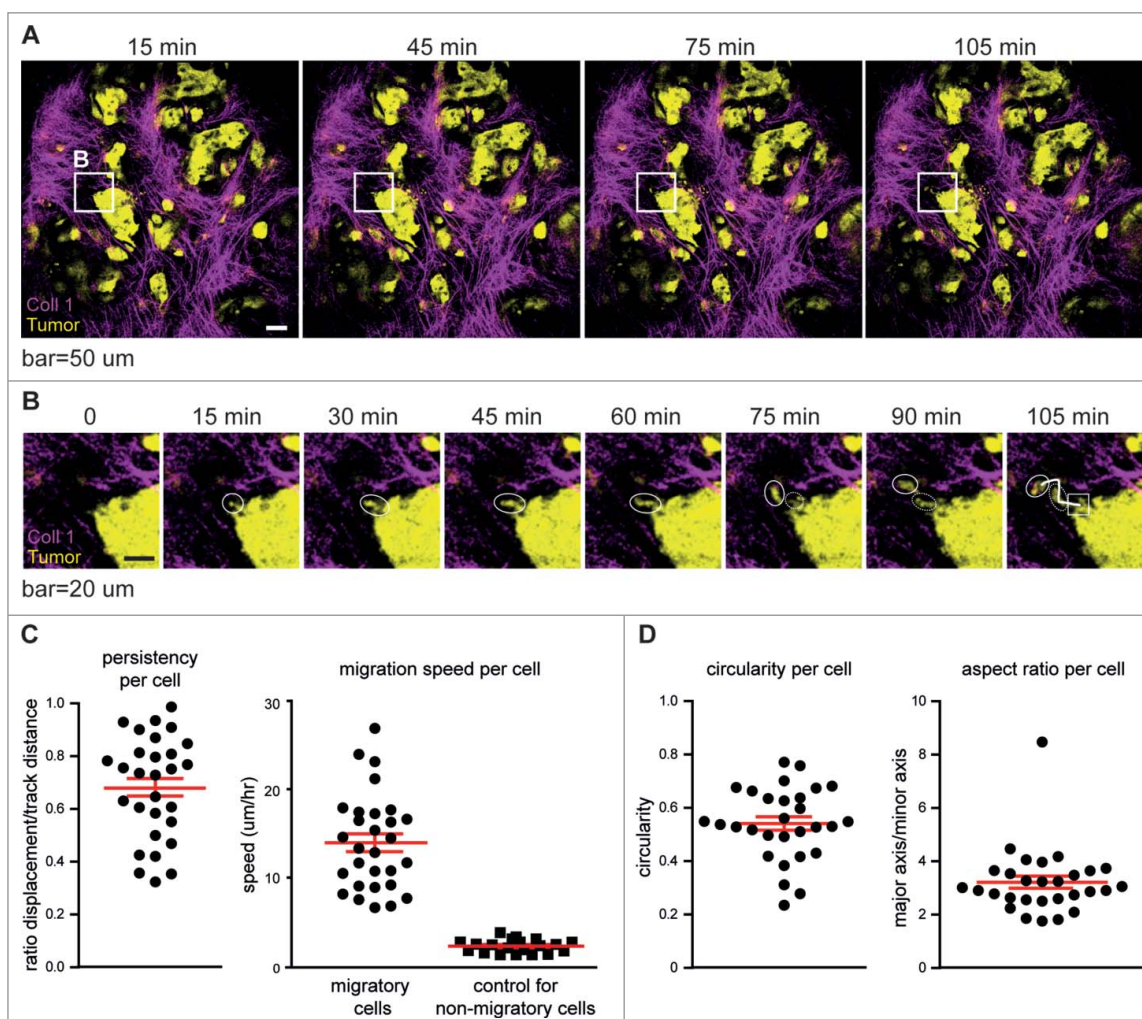
Figure 4. Collective streaming of tumor cells in pancreatic carcinoma. Time-lapse intravital imaging of a genetic fluorescent mouse model of pancreatic cancer with tumor cells shown in yellow and collagen I in magenta. (A) Example of an imaging field (showing 4 time points (30 minute interval)), in which a collective stream of polar and elongated single tumor cells was observed (boxed area is enlarged in B). Scale bar, 50 μm. (B) Boxed area in a showing a collective stream of polar and elongated single tumor cells with a track (last timepoint, white line). Scale bar, 20 μm. (C) The persistency (left graph) and migration speed (right graph) are plotted for every migrating tumor cell. As a control the speed of non-migratory cells are shown (right graph). (D) The circularity (left graph) and aspect ratio (right graph) are plotted for every migrating tumor cell.

metastasis formation we need to focus on studying the micro-environmental cues that lead to cell motility. Moreover, our study shows that IVM of primary pancreatic tumors in GEMMs represents a powerful tool to study the role of genetic modifications that lead to more or less cellular motility and to test new therapies that target cell migration.

Materials and methods

Mice

Experiments were performed with pdx-1-Cre;Kras$^{+/+}$; Trp53$^{\text{LSL-R172H/FLOX}}$;Rosa26$^{\text{YFP/+}}$ (KP$^{\text{F/M}}$C-YFP) mice on a mixed background. The genotype gives rise to

YFP-expressing pancreatic tumors. Mice were housed under standard laboratory conditions and received food and water ad libitum. All experiments were performed in accordance with the guidelines of the Animal Welfare Committee of the Royal Netherlands Academy of Arts and Sciences, The Netherlands and the Animal Welfare Committee of the University Medical Center Utrecht, The Netherlands. Tumor development in KP$^{\text{F/M}}$C-YFP mice is comparable with tumor development in the KP$^{\text{F/M}}$C model for accelerated pancreatic tumor growth[15] showing an average of 20 percent tumor area of the total pancreas on day 30 after birth, increasing to an average of 90 percent on day 51. These mice show a median survival of 63 d.

For the intravital imaging experiments, $KP^{F/M}C$-YFP mice were used at 49–54 d of age to minimize the chance of losing mice during imaging procedures because of excessive tumor growth or presence of ascites impeding imaging.

Intravital imaging

Before imaging, some mice received an intravenous injection of a mix of 90 ul 70 k_D Texas Red Dextran (10 mg/ml, Invitrogen) and 10 ul Hoechst (25 mg/ml, Sigma) to visualize blood vessels and cell nuclei, respectively. Mice were sedated using isoflurane inhalation anesthesia (1.5% to 2% isoflurane/O_2 mixture). The pancreas was surgically exposed, after which the imaging site was cleared of ascites if present. The mouse was then placed with its head in a facemask within a custom designed imaging box. The isoflurane was introduced through the facemask, and ventilated by an outlet on the other side of the box. The pancreatic tumor area was kept moist by surrounding the pancreas by gauze soaked in PBS and covering the surgically exposed part of the mouse with parafilm to prevent dehydration. The mouse received 100 μl PBS subcutaneously and the temperature of the imaging box and microscope were constantly adjusted to keep the mice between 36 and 37°C by a climate chamber that surrounds the whole stage of the microscope including the objectives. Imaging was performed on an inverted Leica TCS SP5 AOBS multi-photon microscope (Mannheim, Germany) with a chameleon Ti:Sapphire pumped Optical Parametric Oscillator (Coherent Inc. Santa Clare, CA, USA). The microscope is equipped with 2 HyDs and 2 PMT non-descanned detectors: HyD1 (520–550 nm), HyD2 (467–499 nm), NDD3 (565–605 nm), NDD4 (SHG). YFP and Texas Red Dextran were excited at 960 nm, YFP was detected in HyD1, Texas Red Dextran was detected in NDD3. Second harmonic generation was detected in HyD2 at 960 nm. Hoechst was excited at 780 nm and detected in HyD2. Images were acquired every 15 minutes for at least 2 hours as Z-stacks with 3 μm step sizes. All images were collected in 12 bit and acquired with a 25x (HCX IRAPO N.A. 0.95 WD 2.5 mm) water objective.

Imaging analysis and quantification

All images were processed using ImageJ software; pictures were converted to RGB, smoothed (if necessary), cropped (if necessary), rotated (if necessary) and contrasted linearly. Videos were corrected for XY and Z drift using custom-written software (codes on request available from J.v.R.). Imaging positions showing migrating tumor cells were selected and migrating tumor cells were counted manually. The center of cells was tracked using ImageJ software and cells that migrated more than one cell diameter over the entire time lapse were selected for further analysis. Velocity was calculated by dividing the total track distance by the total time, persistency was calculated by dividing the total displacement by the total track distance. Circularity was measured using ImageJ by manually drawing a ROI around the tracked cells at 2 or 3 time points and performing 'shape descriptors' measurements (4π x (area/(perimeter^2)). This describes the value between 0 and 1, where 1 indicates a perfect circle. The average circularity of the 2 or 3 time points was used for the tracked cells. The aspect ratio of cells was calculated by measuring the length of the major axis and minor axis and dividing these to get a ratio. A perfect circle has an aspect ratio of 1. A cell with an aspect ratio of less than 2 was considered amoeboid.[24,27–30] The average aspect ratio of 2 or 3 time points (same time points as used for measuring circularity) was used for the tracked cells. 3D reconstructions were created using Imaris 8.3 software (Bitplane).

Tumor processing

Tumors were isolated from the mice at the end of the experiment, a part of every tumor was cut into $\sim$2×2 mm pieces and frozen in freezing medium (10% DMSO/60% fetal calf serum/30% DMEM/F12 + GlutaMAX (GIBCO, Invitrogen Life Technologies)) for transplantation purposes (see 'Tumor cell injection into the pancreas'). The remaining parts of the tumors were fixed in periodate-lysine-paraformaldehyde (PLP) buffer (2.5 ml 4% paraformaldehyde + 0.0212 g $NaIO_4$ + 3.75 ml L-Lysine + 3.75 ml P-buffer (81 ml of 0.2 M Na_2HPO_4 and 19 ml of 0.2 M NaH_2PO_4 added to 100 ml demi water (pH 7.4))) O/N at 4°C to preserve fluorescence. The following day, the fixed tumors and tissues were washed twice with P-buffer and placed for at least 6 hours in 30% sucrose at 4°C. The tumors were then embedded in OCT tissue freezing medium (Leica Microsystems, Nussloch, Germany) and stored at −80°C.

Immunohistochemistry

H&E and Sirius Red stainings were performed on 6 μm OCT-embedded sections. 0.5 g of Sirius Red (Direct Red 80, Sigma) was dissolved in 500 ml saturated aqueous solution of picric acid (1.3% in water) (Sigma) and used to stain collagen. Imaging was performed on a Leica DM4000 B LED microscope equipped with a Leica DFC450 Digital Camera. Images were acquired using Leica LAS-X software.

Fluorescence imaging on YFP- and non-fluorescent tumor sections

Six um slices of frozen tumors (see 'Tumor processing') with and without YFP expression were cut and dehydrated overnight at room temperature in the dark, followed by rehydration in PBS for 10 minutes and mounting with Vectashield Hard set with DAPI (Vector Labs). Imaging was performed with exactly the same settings as described above (see ' Intravital imaging').

Statistical analysis

All data was expressed as mean and standard error of the mean (SEM). Mean and SEM were calculated using Graphpad software or Excel.

Abbreviations

EMT	epithelial-to-mesenchymal transition
GEMMs	genetically engineered mouse models
IVM	Intravital microscopy
KP$^{F/M}$C	pdx-1-Cre; Kras$^{LSL-G12D/+}$; Trp53$^{LSL-R172H/FLOX}$
KP$^{F/M}$C-YFP	pdx-1-Cre; Kras$^{LSL-G12D/+}$; Trp53$^{LSL-R172H/FLOX}$; Rosa26$^{YFP/+}$
SEM	standard error of the mean
SHG	second harmonic generation
YFP	yellow fluorescent protein

Disclosure of potential conflicts of interest

No potential conflicts of interest were disclosed.

Acknowledgments

Funding

References

[1] Hingorani SR, Wang L, Multani AS, Combs C, Deramaudt TB, Hruban RH, Rustgi AK, Chang S, Tuveson DA. Trp53R172H and KrasG12D cooperate to promote chromosomal instability and widely metastatic pancreatic ductal adenocarcinoma in mice. Cancer Cell 2005; 7:469-83; PMID:15894267; http://dx.doi.org/10.1016/j.ccr.2005.04.023

[2] Olive KP, Jacobetz MA, Davidson CJ, Gopinathan A, McIntyre D, Honess D, Madhu B, Goldgraben MA, Caldwell ME, Allard D, et al. Inhibition of Hedgehog signaling enhances delivery of chemotherapy in a mouse model of pancreatic cancer. Science 2009; 324:1457-61; PMID:19460966; http://dx.doi.org/10.1126/science.1171362

[3] Rhim AD, Mirek ET, Aiello NM, Maitra A, Bailey JM, McAllister F, Reichert M, Beatty GL, Rustgi AK, Vonderheide RH, et al. EMT and dissemination precede pancreatic tumor formation. Cell 2012; 148:349-61; PMID:22265420; http://dx.doi.org/10.1016/j.cell.2011.11.025

[4] Zheng X, Carstens JL, Kim J, Scheible M, Kaye J, Sugimoto H, Wu CC, LeBleu VS, Kalluri R. Epithelial-to-mesenchymal transition is dispensable for metastasis but induces chemoresistance in pancreatic cancer. Nature 2015; 527:525-30; PMID:26560028; http://dx.doi.org/10.1038/nature16064

[5] Ellenbroek SI, van Rheenen J. Imaging hallmarks of cancer in living mice. Nat Rev Cancer 2014; 14:406-18; PMID:24854083; http://dx.doi.org/10.1038/nrc3742

[6] Hanahan D, Weinberg RA. Hallmarks of cancer: the next generation. Cell 2011; 144:646-74; PMID:21376230; http://dx.doi.org/10.1016/j.cell.2011.02.013

[7] Beerling E, Ritsma L, Vrisekoop N, Derksen PW, van Rheenen J. Intravital microscopy: new insights into metastasis of tumors. J Cell Sci 2011; 124:299-310; PMID:21242309; http://dx.doi.org/10.1242/jcs.072728

[8] Fein MR, Egeblad M. Caught in the act: revealing the metastatic process by live imaging. Dis Model Mech 2013; 6:580-93; PMID:23616077; http://dx.doi.org/10.1242/dmm.009282

[9] Valastyan S, Weinberg RA. Tumor metastasis: molecular insights and evolving paradigms. Cell 2011; 147:275-92; PMID:22000009; http://dx.doi.org/10.1016/j.cell.2011.09.024

[10] Sahai E. Mechanisms of cancer cell invasion. Curr Opin Genet Dev 2005; 15:87-96; PMID:15661538; http://dx.doi.org/10.1016/j.gde.2004.12.002

[11] Friedl P, Locker J, Sahai E, Segall JE. Classifying collective cancer cell invasion. Nat Cell Biol 2012; 14:777-83; PMID:22854810; http://dx.doi.org/10.1038/ncb2548

[12] Hezel AF, Kimmelman AC, Stanger BZ, Bardeesy N, Depinho RA. Genetics and biology of pancreatic ductal

adenocarcinoma. Genes Dev 2006; 20:1218-49; PMID:16702400; http://dx.doi.org/10.1101/gad.1415606

[13] Rosenblum WI. Histopathologic clues to the pathways of neuronal death following ischemia/hypoxia. J Neurotrauma 1997; 14:313-26; PMID:9199397; http://dx.doi.org/10.1089/neu.1997.14.313

[14] Almoguera C, Shibata D, Forrester K, Martin J, Arnheim N, Perucho M. Most human carcinomas of the exocrine pancreas contain mutant c-K-ras genes. Cell 1988; 53:549-54; PMID:2453289; http://dx.doi.org/10.1016/0092-8674(88)90571-5

[15] Oosterom I, van Amersfoort M, Szuhai K, Lockley M, Offerhaus JG, Voest E, et al. Gemcitabine-induced invasion of pancreatic ductal adenocarcinoma in an accelerated genetically engineered Kras/P53 mouse model. submitted

[16] Ritsma L, Steller EJ, Ellenbroek SI, Kranenburg O, Borel Rinkes IH, van Rheenen J. Surgical implantation of an abdominal imaging window for intravital microscopy. Nat Protoc 2013; 8:583-94; PMID:23429719; http://dx.doi.org/10.1038/nprot.2013.026

[17] Scheele CLGJ, Maynard C, Van Rheenen J. Intravital insights into heterogeneity, metastasis, and therapy response. Trends in Cancer in press

[18] Condeelis J, Singer RH, Segall JE. The great escape: when cancer cells hijack the genes for chemotaxis and motility. Ann Rev Cell Dev Biol 2005; 21:695-718; PMID:16212512; http://dx.doi.org/10.1146/annurev.cellbio.21.122303.120306

[19] Beerling E, Seinstra D, de Wit E, Kester L, van der Velden D, Maynard C, Schäfer R, van Diest P, Voest E, van Oudenaarden A, et al. Plasticity between Epithelial and Mesenchymal States Unlinks EMT from Metastasis-Enhancing Stem Cell Capacity. Cell Rep 2016; 14 (10):2281-8; PMID:26947068; http://dx.doi.org/10.1016/j.celrep.2016.02.034

[20] Pegtel DM, Ellenbroek SI, Mertens AE, van der Kammen RA, de Rooij J, Collard JG. The Par-Tiam1 complex controls persistent migration by stabilizing microtubule-dependent front-rear polarity. Curr Biol 2007; 17:1623-34; PMID:17825562; http://dx.doi.org/10.1016/j.cub.2007.08.035

[21] Giampieri S, Manning C, Hooper S, Jones L, Hill CS, Sahai E. Localized and reversible TGFbeta signalling switches breast cancer cells from cohesive to single cell motility. Nat Cell biol 2009; 11:1287-96; PMID:19838175; http://dx.doi.org/10.1038/ncb1973

[22] Wyckoff JB, Jones JG, Condeelis JS, Segall JE. A critical step in metastasis: in vivo analysis of intravasation at the primary tumor. Cancer Res 2000; 60:2504-11; PMID:10811132

[23] Condeelis J, Segall JE. Intravital imaging of cell movement in tumours. Nat Rev Cancer 2003; 3:921-30; PMID:14737122; http://dx.doi.org/10.1038/nrc1231

[24] Bzymek R, Horsthemke M, Isfort K, Mohr S, Tjaden K, Muller-Tidow C, Thomann M, Schwerdtle T, Bähler M, Schwab A, et al. Real-time two- and three-dimensional imaging of monocyte motility and navigation on planar surfaces and in collagen matrices: roles of Rho. Sci Rep 2016; 6:25016; PMID:27122054; http://dx.doi.org/10.1038/srep25016

[25] Zanier ER, Fumagalli S, Perego C, Pischiutta F, De Simoni MG. Shape descriptors of the "never resting" microglia in three different acute brain injury models in mice. Intensive Care Med Exp 2015; 3:39; PMID:26215806; http://dx.doi.org/10.1186/s40635-015-0039-0

[26] Yu H, Tay CY, Leong WS, Tan SC, Liao K, Tan LP. Mechanical behavior of human mesenchymal stem cells during adipogenic and osteogenic differentiation. Biochem Biophys Res Commun 2010; 393:150-5; PMID:20117089; http://dx.doi.org/10.1016/j.bbrc.2010.01.107

[27] Zaman MH, Trapani LM, Sieminski AL, Mackellar D, Gong H, Kamm RD, Wells A, Lauffenburger DA, Matsudaira P. Migration of tumor cells in 3D matrices is governed by matrix stiffness along with cell-matrix adhesion and proteolysis. Proc Natl Acad Sci U S A 2006; 103:10889-94; PMID:16832052; http://dx.doi.org/10.1073/pnas.0604460103

[28] Sanz-Moreno V, Gadea G, Ahn J, Paterson H, Marra P, Pinner S, Sahai E, Marshall CJ. Rac activation and inactivation control plasticity of tumor cell movement. Cell 2008; 135:510-23; PMID:18984162; http://dx.doi.org/10.1016/j.cell.2008.09.043

[29] Huang YL, Tung CK, Zheng A, Kim BJ, Wu M. Interstitial flows promote amoeboid over mesenchymal motility of breast cancer cells revealed by a three dimensional microfluidic model. Integr Biol 2015; 7:1402-11; PMID:26235230; http://dx.doi.org/10.1039/C5IB00115C

[30] Wolf K, Mazo I, Leung H, Engelke K, von Andrian UH, Deryugina EI, Strongin AY, Bröcker EB, Friedl P. Compensation mechanism in tumor cell migration: mesenchymal-amoeboid transition after blocking of pericellular proteolysis. J Cell Biol 2003; 160:267-77; PMID:12527751; http://dx.doi.org/10.1083/jcb.200209006

[31] Friedl P, Hegerfeldt Y, Tusch M. Collective cell migration in morphogenesis and cancer. Int J Dev Biol 2004; 48:441-9; PMID:15349818; http://dx.doi.org/10.1387/ijdb.041821pf

[32] Hirata E, Park D, Sahai E. Retrograde flow of cadherins in collective cell migration. Nat Cell Biol 2014; 16:621-3; PMID:24981633; http://dx.doi.org/10.1038/ncb2995

[33] Wormann SM, Song L, Ai J, Diakopoulos KN, Gorgulu K, Ruess D, Campbell A, Doglioni C, Jodrell D, Neesse A, et al. Loss of P53 Function Activates JAK2-STAT3 Signaling to Promote Pancreatic Tumor Growth, Stroma Modification, and Gemcitabine Resistance in Mice and is Associated With Patient Survival. Gastroenterology 2016; 151:180-93.e12; http://dx.doi.org/10.1053/j.gastro.2016.03.010

[34] Provenzano PP, Cuevas C, Chang AE, Goel VK, Von Hoff DD, Hingorani SR. Enzymatic targeting of the stroma ablates physical barriers to treatment of pancreatic ductal adenocarcinoma. Cancer Cell 2012; 21:418-29; PMID:22439937; http://dx.doi.org/10.1016/j.ccr.2012.01.007